JET–R(98)02

Projection-space methods to take into account Finite Beam-width Effects in Two-dimensional Tomography Algorithms

L C Ingesson, P J Böcker[1], R Reichle[2],
M Romanelli[3], P Smeulders.

JET Joint Undertaking, Abingdon, Oxfordshire, OX14 3EA,
[1]Present address: Technische Universiteit Eindhoven, P.O.Box 513, 5600 MB Eindhoven, The Netherlands.
[2] Present address: CEA Cadarache, 13108 Saint-Paul-lez-Durance, France.
[3] Also at Imperial College, London, SW7 2BZ, UK.

A shortened version of this report has been submitted for publication in
Journal of the Optical Society of America A

March 1998

ABSTRACT

Detection systems used for computerized tomography are often approximated by line integrals, despite having non-negligible beam widths due to a finite detector size and a finite acceptance angle. Ways to take into account these beam widths in algorithms for two-dimensional straight-line emission tomography are discussed. It is shown that the full three-dimensional imaging properties of the detection system, including filter functions, can be described in projection space. The relationships with the geometric matrix and étendue, and the application to the Cormack and Iterative Projection-space Reconstruction methods are discussed. Two techniques to compensate for most of the beam-width effects have been developed, which can be combined with many tomography algorithms. The two techniques are demonstrated to improve the quality of tomographic reconstructions of measurements by the bolometer tomography system on the JET (Joint European Torus) tokamak. The strengths and limitations of the methods are discussed.

1. INTRODUCTION

Physical detection systems for tomography have a finite detector surface and a finite acceptance angle. The combination of these finite sizes results in what we will call "finite beam widths." The actual sizes are a trade-off between response (signal-to-noise ratio) and the required resolution. Many tomography algorithms assume the measurements to be along infinitely thin lines, which can result in the blurring of the image, or worse, an incorrect interpretation of the measurements, if structures exist that are of the size of the beam widths. Although in the past several ways have been developed to take into account beam widths, most have a limited applicability to specific problems. For example, deconvolution[1-8] is mainly applicable in detection systems with regular spacing between lines of sight (we will use the term line of sight even when it has a finite width), and when the reconstruction is made in Fourier space. A description of how to take into account "elliptical" beams has been given by Bates and McDonnell.[9] The detection system properties are usually only approximated and assumed to be identical for all detectors. Other methods, such as the geometric function, are limited to series-expansion tomography algorithms. This paper studies the beam-width effects of three-dimensional detection systems for two-dimensional (emission) tomography and proposes algorithms, that do not require regular coverage, to improve the line-integral approximation. It is assumed that effects from re-absorption, refraction, diffraction, and scattering are negligible.

A finite beam width results in an averaging or blurring of features compared with what would have been measured along thin lines. Our main concern is not to restore all features that have been lost by the averaging process of the finite beam width, but to correctly take into account the imaging properties. This is particularly useful when there are steep gradients in the object, or localized peaks. This leads to a *de-blurring* of the image, but not necessarily to a *restoration* of all structures with high spatial frequency. Restoration is only possible if the spacing

between lines of sight is significantly smaller than the beam width (see Bracewell[1]). Our description of properties of detection systems can also be applied in the deconvolution methods to take into account the beam widths.

The aim of the paper is two-fold. Firstly, in Sec. 2 a formalism is derived to fully describe the three-dimensional properties of detection systems for two-dimensional tomography. This formalism is in projection space, because projection space is natural for many tomography algorithms. The relationship of the coverage of *projection space* by a detector and the geometric function describing the imaging properties in *reconstruction space* is shown. The approximation by line integrals is discussed on basis on the conservation of the étendue of the imaging detection system. Secondly, in Sec. 3 two variations of one method are described that compensate for some beam-widths effects in tomography algorithms that assume pure line integrals. In Sec. 4 examples are given of the application of the algorithms and the results are discussed. General conclusions are drawn in Sec. 5.

The application of the algorithms and the properties of detection systems in projection space are illustrated with the bolometer tomography system[10] on the JET (Joint European Torus) tokamak, a device for nuclear fusion research. Some of the bolometers are pin-hole cameras (i.e. several detectors share one aperture), whereas other ones have collimators. The emission profiles expected in a tokamak plasma are strongly asymmetric, which, in combination with the limited access, determines the lay-out of lines of sight. The number of lines of sight (118) is limited by the high cost of detectors and the access to the tokamak.

2. FINITE BEAM-WIDTH EFFECTS IN PROJECTION SPACE AND THE APPROXIMATION BY LINE INTEGRALS

A. The tomography problem

The Radon transform R is a straight-line integral transform that maps functions g with a compact support in $\mathbb{R}^2$ (i.e. zero outside a certain closed region with maximum radius a) onto functions f in a space M:

$$f(p,\xi) = [Rg](x,y) = \iint g(x,y)\,\delta(p + (x - x_0)\sin\xi - (y - y_0)\cos\xi)\,\mathrm{d}x\,\mathrm{d}y, \qquad (1)$$

where the coordinates p and ξ in M parametrize each line of sight; p being the (signed) distance from the origin (x_0, y_0) to the line and the angle of the line with the (horizontal) x axis. The space M is referred to as projection space and has the shape of a Möbius band with width $2a$ and "inverted" periodicity π: $p = [-a, a]$ and $f(p, \xi + \pi) = f(-p, \xi)$, so that $\xi = [0, \pi]$ suffices for a complete description. Many properties of projection space are derived in the literature, see for instance Refs. 11 and 12. To distinguish, the actual space with coordinates x and y is called "reconstruction space." The relationship between the coordinates is:

$$x = x_0 - p\sin\xi + \lambda\cos\xi,$$
$$y = y_0 + p\cos\xi + \lambda\sin\xi,$$

where λ is a parameter indicating distance along the line. Note that the (p,ξ) coordinates depend on the choice of the origin (x_0, y_0). To simplify the expressions we will choose, without loss of generality, (x_0, y_0) = (0,0). Throughout this paper double integrals without limits implicitly imply integration over the entire area.

Solving *g* from a limited number of line-integral measurements *f* is called the tomographic inversion or reconstruction of *f*. We will consider emission tomography, where *g*(*x*,*y*) is the local emissivity of an object. The graphical representation of the function *g*(*x*,*y*) is often called "tomogram" and the representation of $f(p,\xi)$ "sinogram." The latter name reflects the sine shape of $f(p,\xi)$ when $g(x,y)$ is a very localized peak. The sinogram for a typical emission profile in the JET tokamak is shown in Fig. 1(a), where the marked points indicate the lines of sight of the bolometer system.

In physical detection systems the measurements are not exact line integrals, but effects such as the detector size, the width of the viewing chord and the viewing properties out of the reconstruction plane need to be taken into account. The measurements of all discrete detectors are written as the vector $\hat{\boldsymbol{f}}$ (the hat is used to distinguish it from the pure line-integral value). In the following, the subscript *i* will be used to indicate that the quantity is for one physical detector numbered by *i*. A conventional way to take into account the beam widths is by replacing Eq. (1) by

$$\hat{f}_i = \iint K_i(x,y)\, g(x,y)\, \mathrm{d}x\, \mathrm{d}y, \tag{2}$$

for each element *i* of the measurement vector, where $K_i(x,y)$ is the geometric or apparatus function. The geometric function contains all relevant information about the viewing geometry and calibration factors. Because the function K_i acts as a weight it is sometimes referred to as weight function. Equation (2) can be discretized and written in matrix form.

$$\hat{f}_i = \sum_j K_{ij} g_i \tag{3}$$

This is the approach taken in so-called *series-expansion methods* for tomographic reconstruction.[13] Here, K_{ij} is the geometric matrix and the function *g*(*x*,*y*) has been discretized into a one-dimensional vector $\boldsymbol{g}$. Discretization is achieved by expansion of *g*(*x*,*y*) on a basis of (possibly orthonormal) functions *b*:

$$g(x,y) \approx \sum_j g_j b_j(x,y). \tag{4}$$

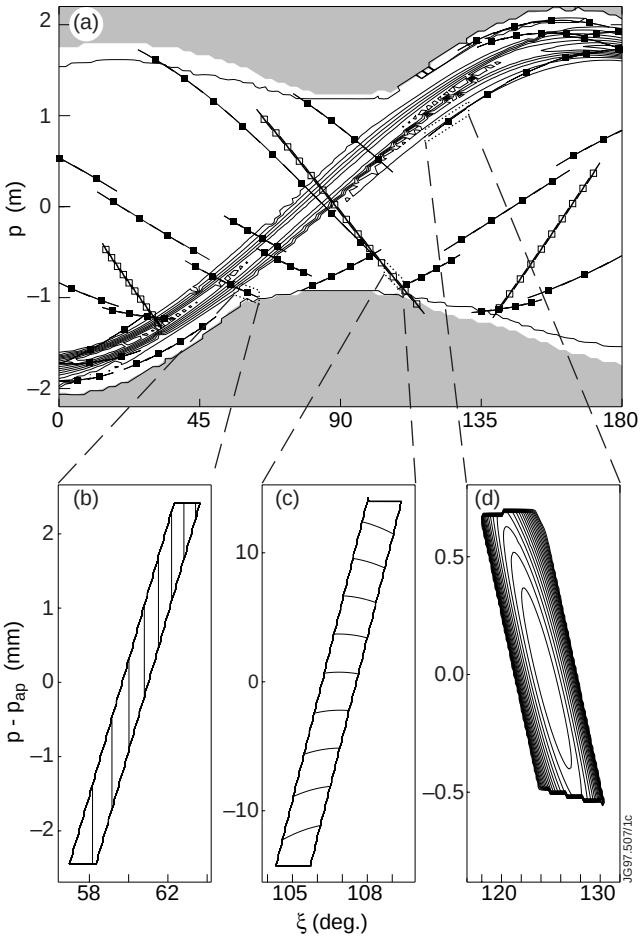

Figure 1. *(a) Contour plot of the sinogram of a typical emission profile in the JET tokamak [calculated from the phantom in Fig. 4(a)]. The origin was chosen on the magnetic axis of the tokamak cross-section. The shaded area indicates where lines of sight pass outside the boundary of the tokamak. The points (solid and open squares) mark the* (p,ξ) *coordinates of the average lines of sight of the JET bolometer system. The regions* D_i *of the detectors are shown around these points (visible only as thin lines). (b-d) Blow up of three regions* D_i *covered by bolometers, where the contours indicate* $k_i(p,\xi)$*: (b) a rectangular pin-hole system with parallel detector and aperture (contours at intervals of 0.2% of the maximum); (c) a rectangular pin-hole system with non-parallel detector and aperture (contours at 0.2% intervals); (d) a system with a rectangular detector, a round collimator, and several other bounding apertures (contours at 5% intervals). In (b-d) the p axis has been stretched by subtracting* $p_{ap}(\xi)$ *[Eq. (23)] corresponding to the centre of the front aperture as a function of* ξ*. In (b) and (c) the maximum contour is in the lower-left corner of the shape, but for detectors straight behind the aperture the maximum is near the middle of the shape.*

The geometric matrix elements are obtained from

$$K_{ij} = \iint K_i(x,y)\, b_j(x,y)\, \mathrm{d}x\, \mathrm{d}y\,. \tag{5}$$

A common discretization of $\boldsymbol{g}$ is into pixels of a grid (see for example Ref. 13), in which case the basis functions b_j are

$$b_j(x,y) = \begin{cases} 1 & \text{if } (x,y) \text{ inside pixel } j, \\ 0 & \text{otherwise.} \end{cases} \tag{6}$$

Another approach to obtain the tomographic reconstruction of f, is to use discretized versions of the analytical inversion formula of Eq. (1). These are called *transform methods*.[14] While it is straightforward to take into account the imaging properties in series-expansion methods by means of the geometric matrix of Eqs. (3) and (5), in general it is more difficult to do so in transform methods. Two methods to do this in an approximate way are described in this paper.

B. The relationship between the geometric function and the coverage of projection space

Due to the finite size of the detector and the finite acceptance angle many rays of light reach each detector. The rays that reach a particular detector form one or more "clouds" of points in projection space (see Fig. 1 and Appendix A). The set of all rays reaching detector i, i.e. rays that are within the entrance pupil of the detection system, will cover a region of projection space designated by D_i. In lossless purely two-dimensional detection systems each ray will contribute fully to the measurement $\hat{f}_i$. However, when there are losses in the optical detection system, e.g. angle-dependent filter effects or contamination of optical surfaces, or effects of the three-dimensional nature of the detection system, a modifying function $k_i(p,\xi)$ has to be placed in front of each line integral $f(p,\xi)$. The total radiation reaching detector i is an integral over all rays D_i that reach that detector:

$$\begin{aligned}\hat{f}_i &= \iint\limits_{D_i} k_i(p,\xi)\, f(p,\xi)\,\mathrm{d}p\,\mathrm{d}\xi = \iint\limits_{D_i}\iint g(x,y)\, k_i(p,\xi)\, \delta(p + x\sin\xi - y\cos\xi)\,\mathrm{d}x\,\mathrm{d}y\,\mathrm{d}p\,\mathrm{d}\xi \\ &= \iint g(x,y) \iint\limits_{D_{i\,i}} k_i(p,\xi)\, \delta(p + x\sin\xi - y\cos\xi)\,\mathrm{d}p\,\mathrm{d}\xi\,\mathrm{d}x\,\mathrm{d}y.\end{aligned} \tag{7}$$

Here, Eq. (1) was used in the second step and the change of integration order in the last step is possible because D_i depends only on the detector, but not on x and y. The integral is independent of the choice of origin (x_0, y_0) of (p,ξ) since the Jacobian is unity for translation and rotation around (x_0, y_0). Comparison of Eq. (7) with Eq. (2) gives as a definition for the geometric function $K_i(x,y)$ for detector i:

$$\begin{aligned}K_i(x,y) &= \iint\limits_{D_i} k_i(p,\xi)\, \delta(p + x\sin\xi - y\cos\xi)\,\mathrm{d}p\,\mathrm{d}\xi \\ &= \int_0^{\pi}\int_{-\infty}^{\infty} k_i(p,\xi)\, \Pi_i(p,\xi)\, \delta(p + x\sin\xi - y\cos\xi)\,\mathrm{d}p\,\mathrm{d}\xi,\end{aligned} \tag{8}$$

where $\Pi_i(p,\xi)$ denotes the window function

$$\Pi_i(p,\xi) = \begin{cases} 0, & (p,\xi) \notin D_i, \\ 1, & (p,\xi) \in D_i. \end{cases}$$

If $k_i(p,\xi) = k$, i.e. constant over the region D_i, as is the case in a lossless purely two-dimensional system, evaluation of Eq. (8) yields

$$K_i(x,y) = k\int_0^{\pi} \Pi_i(-x\sin\xi + y\cos\xi,\xi)\,\mathrm{d}\xi = k\,\Delta\xi, \tag{9}$$

where $\Delta\xi$ is the angle between the points where the curve $p = -x\sin\xi + y\cos\xi$ intersects the boundary of the region where $\Pi_i(p,\xi) = 1$, see Fig. 2. This angle corresponds to the angle spanned by the entrance pupil of the detection system as seen from the point (x,y). To simplify the notation we define $k_i(p,\xi)$ to be zero outside the region D_i so that we can omit $\Pi_i(p,\xi)$. The following properties of $k_i(p,\xi)$ are given for completeness; they are however not used in this paper.

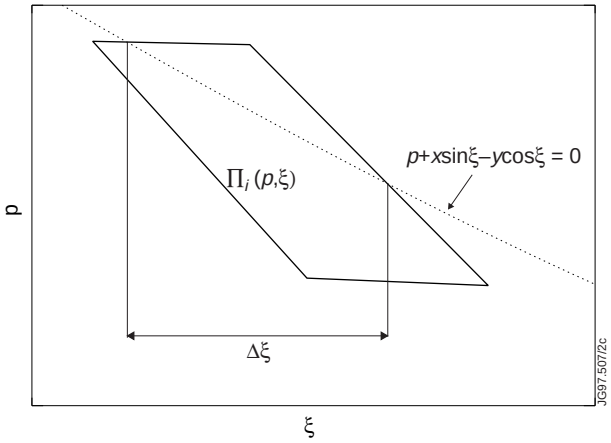

Figure 2. *Interpretation of the angle $\Delta\xi$ of Eq. (9). The thick solid lines indicate the bounds of coverage of projection space of a purely two-dimensional system. The dashed curve corresponds to all lines through a point (*x,y*).*

By inserting the inverse Radon transform (see for instance Ref. 15 for various forms of the Radon inversion formula) for g in Eq. (2) and changing the integration order in a similar way as in Eq. (7), it can be shown that

$$k_i(p,\xi) = -\frac{1}{2\pi^2}\iint \frac{K_i(x,y)}{(p + x\sin\xi - y\cos\xi)^2}\,\mathrm{d}x\,\mathrm{d}y, \tag{10}$$

where the integral is understood in the Cauchy principal value sense. This inversion formula is difficult to use because of the singularity and the fact that $K_i(x,y)$ has to be known in the entire xy plane to fully determine $k_i(p,\xi)$. Although Eq. (10) is of little practical importance, it shows that, in principle, the information contained in $k_i(p,\xi)$ and $K_i(x,y)$ is the same. The information in $k_i(p,\xi)$ is more condensed because it is non-zero in a finite region in projection space. However, knowledge of $K_i(x,y)$ in a finite region in reconstruction space is sufficient to fully characterize the detection system for tomography algorithms. Because the information contained in $k_i(p,\xi)$ is the same as in the geometric function *in reconstruction space* $K_i(x,y)$, we will refer to $k_i(p,\xi)$

as the geometric function *in projection space*.

When $k_i(p,\xi)$ is shift-invariant for all detectors, i.e. $k_i(p,\xi) = k(p-\bar{p}_i, \xi-\bar{\xi}_i)$, it follows, using the same steps as in Eq. (7), that

$$\hat{f}_i = \hat{f}(\bar{p}_i,\bar{\xi}_i) = \iint k(p-\bar{p}_i, \xi-\bar{\xi}_i)\, f(p,\xi)\,\mathrm{d}p\,\mathrm{d}\xi = \iint \tilde{K}(\bar{p}_i,\bar{\xi}_i \mid x,y)\, g(x,y)\,\mathrm{d}x\,\mathrm{d}y, \qquad (11)$$

with $\tilde{K}(\bar{p}_i,\bar{\xi}_i|x,y) = \iint k(p-\bar{p}_i,\xi-\bar{\xi}_i)\,\delta(p+x\sin\xi-y\cos\xi)\,\mathrm{d}p\,\mathrm{d}\xi$, which is related to the point-spread function in optics. Because of the convolution in Eq. (11), f can be found from $\hat{f}$ by deconvolution, which is the basis of some of the deconvolution methods for beam-width correction mentioned in the introduction (where generally the geometric transfer function, i.e. the Fourier transform of the point-spread function, is used). This paper, however, is concerned with the more general case where $k_i(p,\xi)$ can be very different for different detectors. It is important to realise that Eq. (7) assigns a discrete value $\hat{f}_i$ to *regions* of projection space, whereas Eqs. (1) and (11) assign a value to every point of projection space [hence the final step in Eq. (11) can be seen a generalization of Eq. (1) for certain types of physical detector configurations].

C. Étendue in two dimensions

To determine quantities that are required for the approximation of an actual detection system by a line integral, such as the average viewing direction and a scaling factor, it is relevant to examine line integrals of $K_i(x,y)$ along lines that do not pass through the entrance pupil of the detection system. We parametrize such a line $\boldsymbol{L}$ as

$$\boldsymbol{L}(s) = \begin{pmatrix} x(s) \\ y(s) \end{pmatrix} = \begin{pmatrix} x_1 + s\,x_\mathrm{d} \\ y_1 + s\,y_\mathrm{d} \end{pmatrix},$$

where (x_1,y_1) is a starting point on the line and $(x_\mathrm{d},y_\mathrm{d})$ the direction vector. The line integral along this line is

$$\begin{aligned} \int_L K_i(x(s),y(s)) \left\| \frac{\mathrm{d}\boldsymbol{L}(s)}{\mathrm{d}s} \right\| \mathrm{d}s &= \int_{-\infty}^{\infty}\int_0^{\pi}\int_{-\infty}^{\infty} k_i(p,\xi)\,\delta(p+x(s)\sin\xi - y(s)\cos\xi)\sqrt{x_d^2+y_d^2}\,\mathrm{d}p\,\mathrm{d}\xi\,\mathrm{d}s \\ &= \int_0^{\pi}\int_{-\infty}^{\infty} \sqrt{x_d^2+y_d^2}\; k_i(p,\xi) \int_{-\infty}^{\infty} \delta(p+x_1\sin\xi - y_1\cos\xi + s[x_\mathrm{d}\sin\xi - y_\mathrm{d}\cos\xi])\,\mathrm{d}s\,\mathrm{d}p\,\mathrm{d}\xi \qquad (12) \\ &= \int_0^{\pi}\int_{-\infty}^{\infty} \frac{\sqrt{x_d^2+y_d^2}}{\left|x_\mathrm{d}\sin\xi - y_\mathrm{d}\cos\xi\right|} k_i(p,\xi)\,\mathrm{d}p\,\mathrm{d}\xi = E_i(x_\mathrm{d},y_\mathrm{d}). \end{aligned}$$

Here, in the first step Eq. (8) was substituted, and the following property for delta functions was used in the final step

$$\int_{-\infty}^{\infty} f(z)\,\delta(a+bz)\,\mathrm{d}z = \frac{1}{|b|} f(-\tfrac{a}{b}),$$

with, in this case, $f(x) \equiv 1$. If the line $\boldsymbol{L}$ passes through the entrance pupil of the detection system the result of Eq. (12) is not finite.

Because the result $E_i(x_\mathrm{d}, y_\mathrm{d})$ in Eq. (12) is independent of (x_1, y_1), it shows that all integrals of K_i along parallel lines give the same result. Assuming a uniform emission from a strip in direction $(x_\mathrm{d}, y_\mathrm{d})$ with width dl, Fig. 3 shows that the effective thickness of the strip for the line (p,ξ) is

$$\frac{\mathrm{d}l}{\cos\alpha} = \frac{\sqrt{x_\mathrm{d}^2 + y_\mathrm{d}^2}}{x_\mathrm{d}\sin\xi - y_\mathrm{d}\cos\xi}\,\mathrm{d}l$$

where α is the angle between the normal of the strip and the line (p,ξ) (independent of choice of origin). This explains the factor in front of $k_i(p,\xi)$ in Eq. (12): when the total contribution of the uniformly emitting slab to the detector measurement is calculated with the integral over in projection space according to the result of Eq. (12) the factor corrects for the varying contributions from different lines (p,ξ).

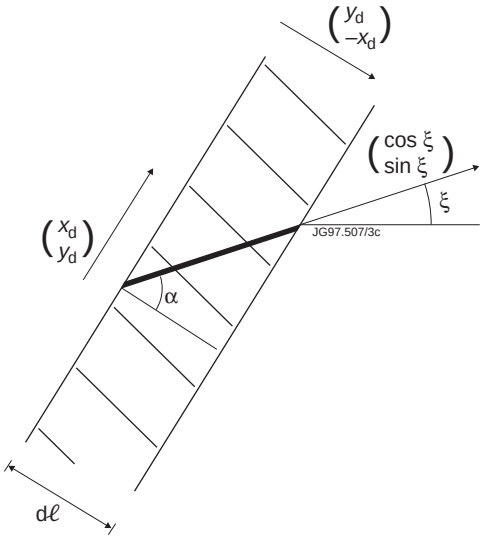

Figure 3. *Geometrical clarification of the factor in front of $k_i(p,\xi)$ in the integrand of the last term of Eq. (12). The symbols are as defined in the text. The factor is seen to stem from the correction of strip thickness by the factor* $\cos\alpha$.

Because in pinhole cameras the rays are not imaged, Eq. (12) shows that the integral along the detector equals the integrals along all planes parallel to it. This result is clearly equivalent to the well-known concept of conservation of étendue or throughput of an optical detection system. For three-dimensional systems this will be discussed in more detail in the next subsection. It is also clear that it is sufficient that the integral over *s* in Eq. (12) extends over the entire length of the line *L* from which there are contributions to the detector, i.e. inside the viewing cone.

D. Extension to the third dimension

One purpose of this paper is to show how three-dimensional properties of detection systems can be implemented in two-dimensional tomography. Two-dimensional tomography is only possible if the variation in the third dimension of the object studied is negligible over the width measured by the system. We will assume that $g(x,y,z) = g(x,y)$, i.e. there is no variation in the third direction *z*. If this is not the case, but the variation in the *z* direction is known *a priori*, the methods described in this article might still be partly applicable or the geometric function in reconstruction space $K_i(x,y)$ can be calculated and used in a tomographic series-expansion method by solving Eq. (3).

To extend the formalism developed in the previous subsections to three dimensions it must be shown that all properties of the third dimension of the detection system can be described adequately by the function $k_i(p,\xi)$ of Eq. (7). We introduce a filter function η_i for rays, which is the attenuation of the ray, or zero if this ray does not go through the entrance pupil of the system for detector *i* from the right direction. The ray can be described completely by four parameters, for which we choose p, ξ, z_L and θ. Here, p and ξ are the projection space coordinates for the projection of the ray onto the *xy* plane, θ the angle with the *xy* plane, and z_L is the distance from the *xy* plane to a characteristic point on the line. If we choose z_L at the point where the line (p,ξ) in the *xy* plane has the shortest distance to the origin, then $z_\mathrm{L} = z - (x\sin\xi + y\cos\xi)\tan\theta$ for a line that goes through the point (*x*,*y*,*z*). The solid angle $K_i'(x,y,z)$ spanned by the entrance pupil of the detection system for detector *i* seen from the point (*x*,*y*,*z*), attenuated by a filter function, is

$$K_i'(x,y,z) = \int_0^{\pi}\int_{-\pi/2}^{\pi/2} \eta_i(p(x,y,\xi),\xi,z_\mathrm{L}(x,y,z,\xi,\theta),\theta)\cos\theta\,\mathrm{d}\theta\,\mathrm{d}\xi, \qquad (13)$$

where $\cos\theta$ is the Jacobian of spherical coordinates, and the integral over ξ needs only to be over $[0,\pi]$ instead of over $[0,2\pi]$ because η_i for rays going through the entrance pupil from the wrong direction is zero, but ξ is the same for both directions. The two-dimensional geometric function in reconstruction space is obtained by integration over *z*:

$$K_i(x,y) = \int_{-\infty}^{\infty} K_i'(x,y,z)\,\mathrm{d}z = \int_0^{\pi}\int_{-\infty}^{\infty}\int_{-\pi/2}^{\pi/2} \eta_i(p(x,y,\xi),\xi,z_\mathrm{L}(x,y,z,\xi,\theta),\theta)\cos\theta\,\mathrm{d}\theta\,\mathrm{d}z\,\mathrm{d}\xi, \qquad (14)$$

where in the second step the integration order has been changed. In Eq. (14) z can be substituted by z_L without changing the integrand nor the integration range. The resulting innermost two integrals therefore only depend on p and ξ, and, substituting $p = -x\sin\xi + y\cos\xi$, comparison of Eq. (14) with Eq. (8) shows that the innermost integrals correspond to the function $k_i(p,\xi)$, which can therefore be calculated by

$$k_i(p,\xi) = \iint \eta_i(p,\xi,z,\theta)\cos\theta \,\mathrm{d}\theta\,\mathrm{d}z. \tag{15}$$

In a simple pinhole system without filter $k_i(p,\xi)$ can be calculated analytically, see Appendix A. Examples of the function $k_i(p,\xi)$ for three bolometer detectors at JET are shown in Figs. 1(b-d).

It has been shown that for arbitrary three-dimensional detection systems a function k_i exists that depends only on p and ξ. Therefore, the validity of Eq. (12) has been extended to the third dimension, which proves that all integrals of $K'(x,y,z)$ over parallel planes will give the same value. This integral of solid angle over an area is usually called étendue or throughput in the literature about optical systems, see for example Ref. 16. Its conservation through lossless optical systems is a well-known concept. The étendue is the quantity that is required to approximate a measurement by a line integral. When the optical system is not imaging (rays go straight through, as in pinhole systems) the étendue is conserved on both sides of the imaging system (if the medium is the same on both sides), i.e. the étendue calculated over the detector is the same as over all planes parallel to it. This is also the case for imaging systems in the geometrical optics approximation (taking into account the magnification), but not in systems where the imaging plane is curved. In emission tomography we only need to consider the étendue of planes in the emitting object, where it is conserved if the medium is non-absorbing and nonrefractive.

E. Approximation by line integrals

Because the étendue is conserved in parallel planes, the contribution of each plane to the detector signal will be equal if the emission is constant on planes (inside the viewing cone). This is trivial for an infinitesimally small viewing cone, because the area of the plane increases with l^2, whereas the solid angle spanned by the entrance pupil decreases with l^{-2}, where l is the distance to the detection system. The previous sections have shown that this property is exact also for finite-sized systems. When the emission is constant over surfaces (say perpendicular to the x direction) within the viewing cone, the measurement can be approximated by a line integral as follows

$$\hat{f}_i = \iint K_i(x,y)\,g(x,y)\,\mathrm{d}x\,\mathrm{d}y = \int g(x)\int K_i(x,y)\,\mathrm{d}y\,\mathrm{d}x = E_i(\xi=0)\int g(x)\,\mathrm{d}x = E_i(0)\,f_i, \tag{16}$$

where Eq. (12) was used in the last step and the parameter of E_i indicates the angle of the direction perpendicular to the plane. Of course, Eq. (16) is true for any direction ξ. This

approximation is much used in tomography. Usually it is assumed that the emissivity is constant perpendicular to the average viewing direction $\overline{\xi}_i$, i.e. $E_i(\overline{\xi}_i)$ should be determined. The definition of the average line of sight is not trivial in all cases, a matter we will come back to when it is required for the algorithm. Such an definition is impossible if $k_i(p,\xi)$ is nonzero in separated parts of projection space, as can be the case if there are reflections or multiple viewing directions of individual detectors.[17] Therefore, in such a case the approximation by line integrals is impossible.

An approximate E_i for pin-hole systems is given by

$$E_i = \iint \mathrm{d}\Omega\, \mathrm{d}A \approx \Omega_{\mathrm{eff}} A_{\mathrm{eff}}, \tag{17}$$

where Ω_{eff} is the effective solid angle that the aperture spans as seen from the centre of the detector, and A_{eff} is the effective detector area.[18,19] It can be shown that Eq. (17) is the zeroth order term in a Taylor expansion of the étendue (see Appendix A). Second order corrections can be found in Ref. 20. Equation (12) gives as an alternative exact expression for the étendue

$$E_i(\overline{\xi}_i) = \iint \frac{k_i(p,\xi)}{\cos(\xi - \overline{\xi}_i)} \mathrm{d}p\, \mathrm{d}\xi. \tag{18}$$

In many cases the approximation by Eq. (17) can be adequate. When both the aperture and the detector are rectangular and their distance relatively large, Eq. (17) can be correct within 1%. The second order corrections reduce this further. However, when the detection system is more complex, for example multiple apertures with different shapes, it is much harder to approximate the étendue with a simple calculation. In such cases, and when filters are present, Eq. (18) can be used.[21]

F. Calculation of the geometric matrix

The geometric matrix of line integrals is obtained by integrating the basis functions along the line of sight [Eq. (5)]. In the case of pixels [the basis function of Eq. (6)] the matrix contains the lengths of the line of sight through each pixel. In a physical detection system, the geometric matrix, if required for a tomographic reconstruction method, can be determined by calculating the solid angle spanned by the detector seen from points (x, y) convolved with the basis function. This is a cumbersome five-dimensional integral: two integrals in Eq. (5) and three in Eq. (14). This five-dimensional integral can be separated because $k_i(p,\xi)$ depends only on p and ξ. We can therefore calculate $k_i(p,\xi)$ from Eq. (15), a two-dimensional integral, on a grid in (p,ξ) and tabulate these values. Equation (8) can then be used to calculate the geometric function in reconstruction space (a one-dimensional integral), which should be averaged over the basis function by Eq. (5) (a two-dimensional integral). The gain in speed is due to the tabulating of

values of $k_i(p,\xi)$ in grid points in projection space, between which the required value can be found by interpolation because $k_i(p,\xi)$ is usually a smooth function.

3. ALGORITHMS FOR THE APPROXIMATION OF LINE INTEGRALS IN PROJECTION SPACE

Two algorithms have been developed to improve the approximation by line integrals of detection systems with finite beam widths. The first algorithm is an iterative refinement of the average lines of sight and an étendue weighted by a previous tomographic reconstruction. The second algorithm calculates a weighted étendue based on assumptions of the sinogram. The second method is less general than the first, but much faster. The function $k_i(p,\xi)$ can be applied in other ways as well. A way to take into account beam widths by means of the function $k_i(p,\xi)$ in the Cormack reconstruction method,[18,22] which is still applied in tomography of soft x-ray measurements in nuclear fusion research, is described in Appendix B. The beam-widths can be included in a similar way in the Iterative Projection-space Reconstruction method[23]; see Appendix C. If the coverage is regular and $k_i(p,\xi)$ shift-invariant [see Eq. (11)], the Fourier transform of $k_i(p,\xi)$ can be used in deconvolution methods in projection space, such as in Ref. 8, replacing the approximations of the detection geometry used in most references. We do not consider deconvolution methods further in this paper.

A. Iterative refinement of the weighted centre-of-mass and étendue

In many detection systems the best approximate line of sight seems to be obvious, for example the line connecting the centre of the detector with the centre of the pinhole in a pinhole system. In complicated detection systems it is less obvious and we have to define an average line of sight. In general, the contour plot of the geometric function in reconstruction space $K_i(x,y)$ for a particular detector i will have an elongated shape along the "line of sight". The approximate line of sight can be said to be the one along the main axis of this shape. More exactly, it can be defined as being the direction of the main axis of the equivalent ellipse,[24] which gives satisfactory results.[17] This definition in reconstruction space can be assumed to be equivalent to defining the centre-of-mass of the region D_i in projection space to be the average line of sight. Both definitions are *ad hoc*, but they seem to be sound definitions of an average line of sight. However, if the function $g(x,y)$ has steep gradients, and hence also $f(p,\xi)$, a more proper average line of sight should be shifted towards the higher emission side of the slope. Therefore, we postulate that a good average line of sight is given by the weighted centre-of-mass $(\overline{p}_i, \overline{\xi}_i)$ over the region D_i:

$$\overline{p}_i = \frac{\int_0^{\pi}\int_{-\infty}^{\infty} p\ f(p,\xi)\ k_i(p,\xi)\ \mathrm{d}p\mathrm{d}\xi}{\int_0^{\pi}\int_{-\infty}^{\infty} f(p,\xi)\ k_i(p,\xi)\ \mathrm{d}p\mathrm{d}\xi}, \tag{19}$$

and

$$\overline{\xi}_i = \frac{\int_0^{\pi}\int_{-\infty}^{\infty} \xi\, f(p,\xi)\, k_i(p,\xi)\, \mathrm{d}p\, \mathrm{d}\xi}{\int_0^{\pi}\int_{-\infty}^{\infty} f(p,\xi)\, k_i(p,\xi)\, \mathrm{d}p\, \mathrm{d}\xi}. \tag{20}$$

Both in the limit of an infinitely thin line and in the limit of uniform emission (of an object much larger than the beam widths, so that the variation of $f(p,\xi)$ is negligible) Eqs. (19) and (20) yield the expected result.

The function of the étendue is to scale the line integral f_i to the measurement $\hat{f}_i$. The étendue as defined by Eqs. (17) and (18) is only useful if the approximation of Eq. (16) is allowed, i.e. $g(x,y)$ does not vary over the beam width. If this assumption is not valid, we can define a weighted or effective étendue as the ratio:

$$E_{\mathrm{w}i} \approx \frac{\hat{f}_i}{f(\overline{p}_i,\overline{\xi}_i)} = \frac{\iint g(x,y)\, K_i(x,y)\, \mathrm{d}x\, \mathrm{d}y}{\iint g(x,y)\, \delta(\overline{p}_i + x\sin\overline{\xi}_i - y\cos\overline{\xi}_i)\, \mathrm{d}x\, \mathrm{d}y} = \frac{\iint f(p,\xi) k_i(p,\xi)\, \mathrm{d}p\, \mathrm{d}\xi}{f(\overline{p}_i,\overline{\xi}_i)}, \tag{21}$$

where the second step is an expression in reconstruction space and the last step [from Eq. (7)] the equivalent in projection space. The expression in reconstruction space is equivalent to the iterative scaling of measurements by g and the geometric matrix proposed in Ref. 23. Again, this definition gives the expected result in both the limit of an infinitely thin line and in the limit of uniform emission.

The algorithm for the iterative approximation of line integrals is as follows. First a tomographic reconstruction g is made with the unweighted étendue and average $(\overline{p}_i,\overline{\xi}_i)$. The data of which reconstructions are made will be inconsistent if beam widths are important because of the approximations made. Therefore, we try to refine this data based on the sinogram of g. Average weighted $(\overline{p}_i,\overline{\xi}_i)$ coordinates are calculated by Eqs. (19) and (20) using g. The weighted étendue is calculated according to Eq. (21), which is used to determine a better line-integral approximation f from the measurement $\hat{f}_i$. The reconstruction is then carried out again using the new $(\overline{p}_i,\overline{\xi}_i)$ and f_i. This process, using the latest g, is iterated until the tomogram does not change much any more.

It must be stressed that the result will not be exact because we still attempt to approximate a detection system with finite beam widths by line integrals. The limitations in applicability of the method are discussed after the results in Sec. 4. In certain cases it may be better to omit the refinement of $(\overline{p}_i,\overline{\xi}_i)$, necessarily when a tomography algorithm is used that assumes a regular coverage of projection space and cannot cope with small changes in lines of sight. In such a case, Eq. (21) does still give a proper correction to the étendue. However, if the $(\overline{p}_i,\overline{\xi}_i)$ are updated, the weighted étendue has to be updated as well.

B. Approximation by zero-sized aperture

For many actual tomography systems the width of the region D_i in the p direction, which is of the same order as the aperture size, will be smaller than length scales in the sinogram, i.e. the variation of the function $f(p,\xi)$ over the D_i is negligible in the p direction when ξ is kept constant (see for example Fig. 1). This means that it is possible to separate the p and ξ integrals as follows:

$$\iint f(p,\xi)\, k_i(p,\xi)\,\mathrm{d}p\,\mathrm{d}\xi = \int f(p_i(\xi),\xi) \int k_i(p,\xi)\,\mathrm{d}p\,\mathrm{d}\xi. \tag{22}$$

In a pin-hole system, with the aperture in position $(x_{\mathrm{ap},i}, y_{\mathrm{ap},i})$, we can assign this value to the "aperture curve"

$$p_{\mathrm{ap},i}(\xi) = -x_{\mathrm{ap},i}\sin\xi + y_{\mathrm{ap},i}\cos\xi. \tag{23}$$

This means that we approximate the system by a zero-sized aperture. Other choices for a characteristic point of the system are of course possible, such as the centre of the detector. The zero-sized aperture approximation is preferable in systems in which many channels share the same aperture ("fan-beam systems"), as will be discussed in the next subsection.

The advantage of the separation of Eq. (22) is that the integral of $k_i(p,\xi)$ over p can be carried out separately, yielding an "angular étendue" (dimension $\mathrm{m}^2\ \mathrm{rad}$)

$$e_i(\xi) = \int k_i(p,\xi)\,\mathrm{d}p\,. \tag{24}$$

This approximation drastically reduces the calculation time of Eqs. (19–21). If it is too complicated to calculate the function $k_i(p,\xi)$ for a particular system, but a good approximation of $e_i(\xi)$ can be found, this can also be used in the algorithms. In Appendix A examples of the angular étendue for simple pin-hole systems are shown.

If the shape of the region D_i is very narrow along the aperture curve, but has a span in p for certain ξ that is of the order of the scale length of the sinogram, it could be a better choice in the separation in Eq. (22), not to take $p_i(\xi)$, but to introduce new coordinates d and t, where the t runs along the aperture curve and d is locally perpendicular to it. In that case the angular étendue has to be redefined as a function of t. It is possible to define such locally perpendicular coordinates (see Appendix D), but their evaluation is unfortunately cumbersome (involving the solution of integral or differential equations).

C. Simplified algorithm

When the zero-sized aperture approximation is valid and certain assumptions about the sinogram can be made, the method for beam-width correction can be greatly simplified for fan-beam

systems where several detectors share an aperture. This method is based on a beam-width correction applied by Smeulders.[25,26] With some modifications the method is also applicable to parallel beam systems.

We take t as the variable along the aperture curve. In our application we have used $t = \xi$. We assume that along the aperture curve we can *locally* approximate the sinogram by a second order polynomial, i.e. around point (detector) i: $f(t) = a_i t^2 + b_i t + c_i$. If we know the sinogram values in the point i and its neighbour points (f_{i-1}, f_i and f_{i+1}), we can solve the coefficients a_i, b_i and c_i as *linear* functions of f_{i-1}, f_i and f_{i+1} (see Appendix E). It is also possible to choose functions different from second order polynomials, for example higher order polynomials and correspondingly more neighbours, but it is essential for the method that the coefficients be linear functions of the sinogram values in the measurement points. Given the coefficients, the actual measurement $\hat{f}_i$ can be expressed as [Eq. (7)]

$$\begin{aligned}\hat{f}_i &= \iint k_i(p,\xi)\, f(p,\xi)\,\mathrm{d}p\,\mathrm{d}\xi \approx \int e_i(t)\, f(t)\,\mathrm{d}t \\ &= a_i \int t^2 e_i(t)\,\mathrm{d}t + b_i \int t\, e_i(t)\,\mathrm{d}t + c_i \int e_i(t)\,\mathrm{d}t.\end{aligned}$$

Carrying out the integrals over t and making use of the linear expressions of the coefficients a_i, b_i and c_i, we can write (see Appendix E)

$$\hat{f}_{ii} = q_{ii-1} f_{i-1} + q_{ii} f_i + q_{ii+1} f_{i+1}, \tag{25}$$

and consequently

$$\hat{f} = Qf\,, \tag{26}$$

where Q is a band-diagonal matrix. The coefficients have to be changed slightly for edge channels which have only one neighbour. This matrix does only depend on the geometry and the fitting function and not on the measurements or the sinogram, and thus does not change. The matrix can be inverted, giving the corrections to the raw measurements $\hat{f}$ for beam-width effects, which yields approximate line-integral values f that can be used in the tomographic reconstructions. Effectively, the beam-width correction by this method is similar to the deconvolution method, cf. Bracewell.[1]

4. RESULTS

A. Bolometer tomography at JET

The algorithms described in the previous section have been applied to the bolometer tomography system[10] on the JET tokamak, which has large beam widths that differ for different viewing

directions. When the plasma is toroidally symmetric, the JET bolometer system can be assumed to view one poloidal cross-section of the tokamak. In this poloidal plane the emission is strongly asymmetric: a strong peak is located in the so-called divertor region in the bottom of the cross section, which typically is an order of magnitude higher than the bulk emission [see Fig. 4(a) for an example]. The 118 detectors view the plasma from various directions limited by technical constraints, to give a good coverage of both the bulk plasma and the divertor region [lines of sight in the divertor region are also shown in Fig. 4(a), the coverage of projection space is shown in Fig. 1(a)]. The detection systems have been designed such that the full widths of the viewing cones extend roughly to the neighbouring line of sight, with the full-width-half-maximum of neighbouring channels roughly coinciding. The beam widths are relatively large compared to the emitting structures in the plasma and are determined by detector sensitivity and the limited number of lines of sight.

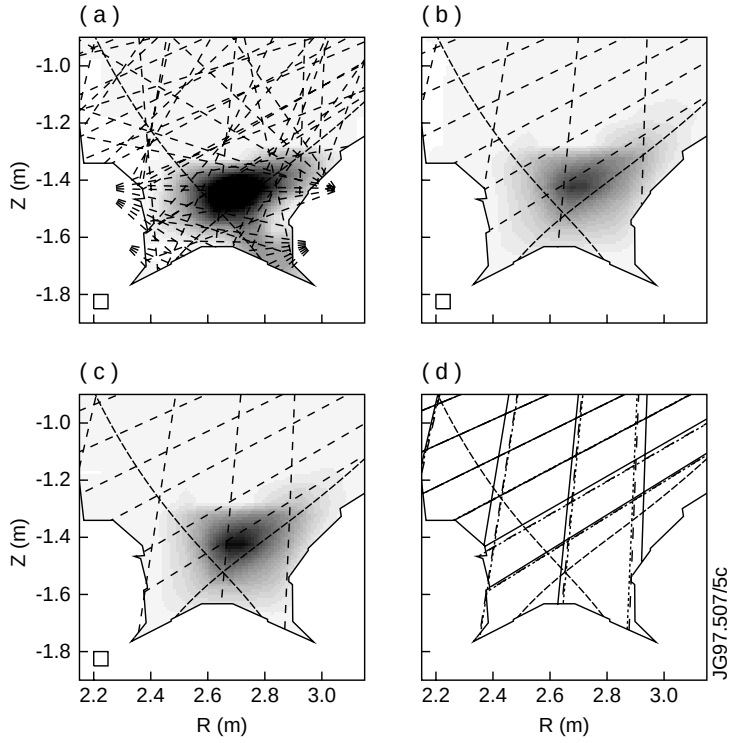

Figure 4. *Grey-scale plots of the emission in the divertor region of a poloidal cross-section of the tokamak (scale: white = 0 W, black = 3 MW). The separatrix, i.e. the last closed flux surface in the tokamak, is shown as a dashed curve for reference. In (a–c) lines of sight are shown as dashed straight lines. The box in the lower left corner indicates the grid size used in the reconstructions. (a) Phantom and the 118 lines of sight. (b) Tomogram of a reconstruction with a reduced number of lines of sight assuming unmodified line integrals (method B). (c) Tomogram of a reconstruction with a reduced number of lines of sight after three iterations of beam-width corrections (method D3). (d) Lines of sight with method D of reconstructions with a limited number of lines of sight during two iterations (solid line: original; dashed line: first iteration; dotted line: second iteration).*

The tomography algorithm applied in the simulations is the one used routinely for both bolometer and soft x-ray tomography at JET.[21,27] It is a series-expansion method with local basis functions, i.e. Eq. (3) is solved, which is suitable for detection systems with irregular coverage. The reconstruction is obtained by a constrained optimization method, where the constraints are (a) that the misfit between measurements and pseudo-measurements calculated from the tomogram be equal to the estimated errors in the measurements, and (b) that the tomogram be positive. The latter constraint is essential due to the peaked emission profile and the relatively sparse coverage with few lines of sight. The regularization used is anisotropic smoothness.[21] The algorithm uses the geometric matrix, so that the beam-width correction algorithms applied with a geometric matrix of line-integrals can be compared with reconstructions that use the actual geometric matrix of the detection system calculated as described in Sec. 2.F.

B. Simulations

The assessment of beam-width correction algorithms has been carried out by means of phantom simulations. Phantoms are pre-described emission profiles which are used to calculate pseudo-measurements, i.e. what would be measured if the phantom were the actual emission profile. A realistic level of noise was added to the pseudo-measurements: Gaussian noise with a standard deviation of 3% of the measurement. Phantom simulations rather than tests with actual measurements are presented because they give more control over the tests without disturbing effects from experimental errors (such as noise and uncertainties in calibration factors and positions), and make it possible to quantify the success of the algorithms by an objective quantifier: the tomogram reconstruction error σ_g. This quantifier measures the relative deviation of the tomogram g from the phantom g_0:

$$\sigma_g = \frac{\|g - g_0\|}{\|g_0\|}.$$

The phantom used, Fig. 4(a), is based on a tomographic reconstruction of actual measurements. Although some structure has been lost in the phantom, it is suitable for our purpose to show the differences between the algorithms.

Two cases are discussed: reconstructions using all 118 lines of sight [all points in Fig 1(a), both solid and open squares], and reconstructions using a reduced number of lines of sight of three fans [open squares in Fig 1(a)]. The quality of the reconstructions of the various algorithms are summarized in Table I. Two sets of simulations are shown for the118 line-of-sight case: one with beam widths for all channels, and one with beam widths for most channels, but not the most difficult ones. The methods compared are: (A) reconstructions with the proper geometric matrix of the detection system; (B) reconstructions using the geometric matrix for line integrals along the average lines of sight (neglecting the weighting by the sinogram); (C) reconstructions of

Table I. *Reconstruction errors σ_g for phantom simulations using various beam-width correction methods. The various cases are referred to by letter in the text. For the first number of the 118-line-of-sight column the beam widths of all lines of sight were used, whereas for the second column some difficult lines of sight were assumed to be pure line integrals in both the pseudo-measurements and the reconstructions. Note that a reconstruction error of 100% only means a large deviation from the phantom, not that the result is completely wrong.*

	σ_g(%)		
Reconstruction type	118 lines of sight		34 lines of sight in 3 fans
A: proper geometric matrix	21.2	23.3	46.3
B: line integrals	29.2	30.6	56.2
C: simplified method	27.5	30.6	54.5
D: 1st iteration of iterative method	23.7	28.4	50.1
D: 2nd iteration of iterative method	25.9	27.9	49.2
D: 3rd iteration of iterative method	26.0	27.5	49.0
E: 1st iteration of iterative method, no change of (p, ξ)	27.8	29.4	51.6

measurements corrected by the simplified method of Sec. 3.C; (D) reconstructions of various iterations of the iterative beam-width correction method (Sec. 3.A) where both the average $(\overline{p}_i, \overline{\xi}_i)$ and étendue are changed; and (E), as D, but without modifying the average $(\overline{p}_i, \overline{\xi}_i)$. Method E was studied because it is relevant for tomography algorithms that do not allow an irregular coverage of projection space. In methods D and E the quantities corrected were weighted with the sinogram of the previous iteration, except in the first iteration where a unity sinogram was assumed. The iterations were stopped when no significant improvement was found compared to the previous iteration. The reconstruction error σ_g is not the only quantifier for the quality of the reconstructions: other ones are the magnitude of artefacts (for example negative values if no non-negativity constraint is applied), and the speed of convergence when the non-negativity constraint is applied. These quantifiers show the same trend as σ_g.

C. Discussion

Methods A and B in Table I are the reference cases: A takes beam widths fully into account; B not at all. Table I shows that the beam-width correction algorithms give an improvement over B in virtually all cases. The improvements in reconstructions obtained by the algorithms for the case of a reduced number of lines of sight are illustrated in Figs 4 (tomograms) and 5 (“cross-sections” of the tomogram along the aperture curve).

The improvement given by the simplified method (method C) is limited, and sometimes not noticeable. This is probably due to the fit by a parabola not being very suitable for this

phantom: although locally the sinogram can be approximated by parabola [see Fig. 5(a)], the coverage is too coarse to support such a fit properly [Fig. 5(b)]. Of course, more suitably chosen fitting functions may perform better. The correction to the étendue can be as large as 20% in the channels observing the peak [see Fig. 5(a)]. In simulations with the soft x-ray tomography system at JET, which has six fans with 35 to 36 channels each, a larger improvement was found.

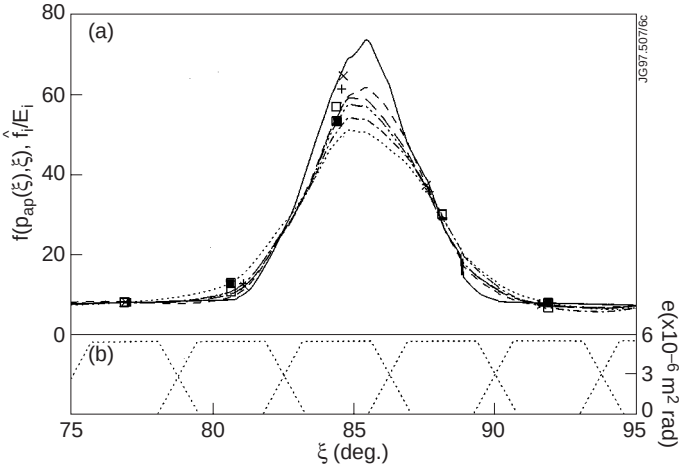

Figure5. *(a) Sinogram values along the aperture curve of the vertical fan for reconstructions with a reduced number of lines of sight. Sinograms of phantom (solid line), reconstructions with the proper geometric matrix (method A: dashed line), line integrals (method B: dotted line), the first and third iteration of the iterative method (D1: dash-dot-dot; D3: long dashes), and the simplified method (C: dash-dot). The symbols indicate: pseudo-measurements divided by the unweighted étendue (filled squares), corrected values by the simplified method (B: open squares), and corrected values in the first and third iteration of the iterative method (D1 and D3: plus sign and cross, respectively). Note the shift in ξ for the points of D1 and D2. (b) For reference, the angular étendue of the relevant channels along the aperture curve.*

The simulations show that the iterative method (D and E) gives significant improvements over method B in both the cases of all and a reduced number of lines of sight. The way the lines of sight change in method D during the iterations is shown in Fig. 4(d), and can also be seen in Fig. 5(a). As expected, the lines of sight move towards the peak emission and make it possible to obtain a de-blurred, more peaked reconstruction. This de-blurring is visible when comparing Fig. 4(b) with Fig. 4(c), and is very clear in Fig. 5(a). In these simulations the corrections to the étendue were up to 5% for most channels and 10% for the channels seeing the peak [see Fig. 5(a)]. In most cases studied, subsequent iterations give improvements for method D, whereas little improvement is found after the first iteration in method E. The simulation with beam widths for all 118 lines of sight in Table I is an exception, where the first iteration of method D is better than subsequent iterations. Method D performs better than method E, but method E can be useful in certain cases. Other simulations, for example for the soft x-ray tomography system at JET, a similar behaviour was found, although the improvements were small due to the less significant beam widths.

The de-blurring effect of taking into account the beam widths has also been observed in reconstructions of actual measurements, in which case they can be even more pronounced. This is probably because the gradients in the actual emission profiles are more pronounced than those in the phantom, which was based on a reconstruction that probably was oversmoothed like all reconstructions with a limited number of lines of sight. The application of the beam-width correction methods on actual measurements are not considered further in this paper because of the lack of an objective quality quantifier.

The simulations show that the beam-width correction algorithms are successful in improving the reconstructions. They also show that for some cases they are more successful than in other ones, depending on the detection system and the emission profile. Therefore, phantom calculations should always be carried out to determine which algorithm improves the result most, before applying the algorithms. Contrary to methods that take into account the full geometry of the system (such as method A), the two proposed algorithms cannot be expected to function properly in detection systems that certainly cannot be approximated by line integrals, for example in systems where individual detectors have multiple viewing directions or when there are reflections or scatter of radiation. Furthermore, the methods cannot be guaranteed to converge. They might not converge when, for example, there are several local peaks smaller than the beams widths, or when the reconstructed emissivities are negative. In many cases, however, when few structures of the size of beam widths are present, both methods can perform well.

5. CONCLUSIONS

It has been shown that the full three-dimensional imaging properties of detection systems for two-dimensional tomography can be described in projection space. This includes filter effects in the detection system (see for example Refs. 17 and 21 for systems with filters). The description in projection space is related to the conservation of the étendue in optical systems. The properties of the detection system in projection space have been used to find approximations of the system by line integrals that are an improvement over the straightforward use of the étendue and the average line of sight. Furthermore, a fast method to calculate the geometric matrix from the coverage of projection space has been indicated.

Two algorithms, based on the detection-system properties in projection space, to correct for beam widths have been proposed and have been shown to work satisfactorily for an actual tomography system. The algorithms are generally applicable to tomography methods that assume pure straight-line integrals in an optically thin medium, and are more general than, for example, correction methods based on deconvolution. Furthermore, the algorithms only modify the geometry and étendues, and can therefore easily be used in combination with existing tomography codes. However, the assumptions made in the algorithms are not always valid, and proper care should be taken when applying them. Taking into account the full geometric matrix of the detection

system, if possible, seems to be preferable. The proposed algorithms can be a solution if that is not possible or the geometric matrix is too complicated to calculate. The algorithms also give a means to assess the importance of beam-width effects.

ACKNOWLEDGEMENTS

The initial work that led to this paper was carried out by one of the authors (LCI) at the FOM-Instituut voor Plasmafysica, Nieuwegein, the Netherlands under the Euratom-FOM association agreement with financial support from NWO and Euratom. The same author would like to thank Prof. V.V. Pickalov for initiating him into tomography methods and the properties of projection space, and for the discussions on the need for scaling of measurements of systems with finite beam widths to line integrals.

APPENDIX A: SOME PROJECTION-SPACE PROPERTIES OF PIN-HOLE SYSTEMS

The description in projection space of a simple pin-hole system with rectangular detector and rectangular aperture is straightforward and some quantities can be expressed analytically. Furthermore, such systems are regularly applied in practice. Therefore, such a system has been chosen to illustrate the coverage of projection space, the angular étendue, the étendue and the geometric functions in reconstruction and projection space.

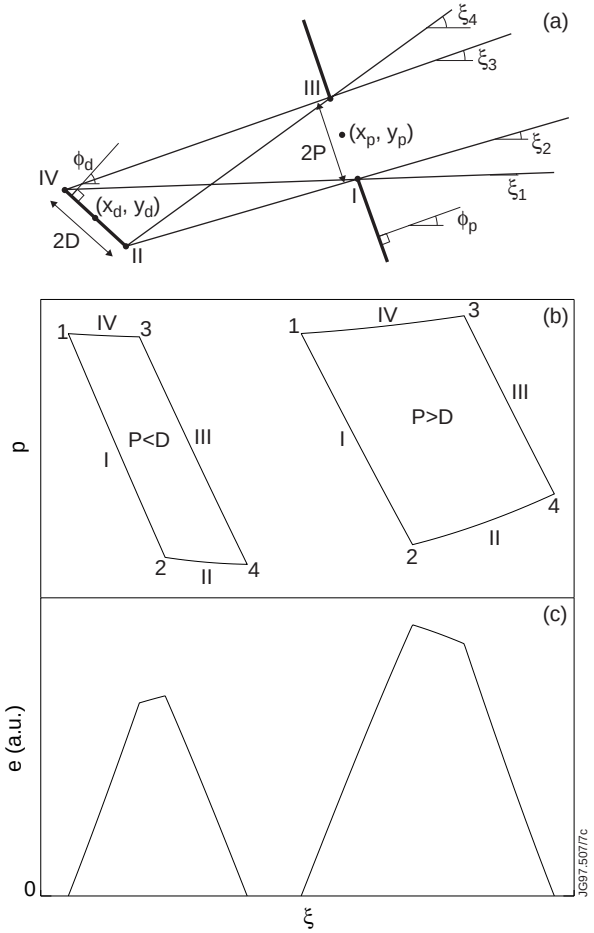

Figure 6. *(a) Geometry in the* xy *plane of the pin-hole system discussed in Appendix A. (b) Boundaries in projection space for two pin-hole systems with varying pinhole size. The detector and aperture were taken parallel. The angles at which the curves start and end are given in Table II. (c) Angular étendues for the systems of (b).*

The geometry of the pin-hole system is shown in Fig. 6(a). It is assumed that the detector and aperture are rectangular and have two edges parallel to the *xy* plane, and that the detector and aperture are perpendicular to the *xy* plane. The boundaries of the region covered in projection space are shown in Fig. 6(b). Two cases are considered: one where the aperture is larger than the detector and vice versa. The coordinates of the bounding points I to IV and the angles are given in Table II. The functions of the boundary curves in Fig. 6(b) are

$$p_h(\xi) = -(x_h - x_0)\sin\xi + (y_h - y_0)\cos\xi, \tag{A1}$$

where h is I … IV and (x_0, y_0) is the origin of the (p,ξ) coordinates. The width of the region in the p direction is related to the aperture size.

TableII. *Bounding points and angles of the pin-hole system shown in Fig. 6.*

Point h	x_h	y_h	ξ range	Angle ε	tan ξ_ε
I	$x_p + P\sin\phi_p$	$y_p - P\cos\phi_p$	$\xi_1 \to \xi_2$	1	$(y_I - y_{IV})/(x_I - x_{IV})$
II	$x_d + D\sin\phi_d$	$y_d - D\cos\phi_d$	$\xi_2 \to \xi_4$	2	$(y_I - y_{II})/(x_I - x_{II})$
III	$x_p - P\sin\phi_p$	$y_p + P\cos\phi_p$	$\xi_4 \to \xi_3$	3	$(y_{III} - y_{IV})/(x_{III} - x_{IV})$
IV	$x_d - D\sin\phi_d$	$y_d + D\cos\phi_d$	$\xi_3 \to \xi_1$	4	$(y_{III} - y_{II})/(x_{III} - x_{II})$

If for a given line (p,ξ) the distance between the points of intersection on the detector and aperture is $L(p,\xi)$, and in the z direction the detector extends between z_d^- and z_d^+, and the aperture between z_p^- and z_p^+, we can calculate

$$\begin{aligned} k(p,\xi) &= \int_{z_d^-}^{z_d^+}\int_{\theta^-}^{\theta^+}\cos\theta\,\mathrm{d}\theta\,\mathrm{d}z \\ &= \sqrt{L^2(p,\xi) + (z_p^+ - z_d^-)^2} - \sqrt{L^2 + (z_p^- - z_d^-)^2} - \sqrt{L^2 + (z_p^+ - z_d^+)^2} + \sqrt{L^2 + (z_p^- - z_d^+)^2}, \end{aligned} \tag{A2}$$

where the z integral is carried out over the detector surface [Eq. (15) shows that any z integral for constant (p,ξ) will give the same result] and we have realised that the bounds of θ are given by $\sin\theta^\pm = (z_p^\pm - z)/\sqrt{L^2(p,\xi) + (z_p^\pm - z)^2}$.

If the detector and aperture are parallel, L will be independent of p, and so will k from Eq. (A2). Therefore, the angular étendue of Eq. (24) can be expressed analytically as

$$e(\xi) = k(\xi)\,\Delta p(\xi),$$

where $\Delta p(\xi)$ is the difference of the curves of Eq. (A1) in the appropriate interval. The angular étendue of the detectors of Fig. 6(b) is shown in Fig. 6(c).

The étendue can be obtained by combining Eqs. (18) and (24), which yields

$$E(\overline{\xi}) = \int \frac{e(\xi)}{\cos(\xi - \overline{\xi})}\,\mathrm{d}\xi.$$

In general, the integrand will be a very complicated function in ξ, and can therefore only be calculated numerically. However, if the detector and aperture dimensions, D and P, are small compared to the perpendicular distance l between the detector and aperture planes, a Taylor expansion in ξ around $\bar{\xi}$, and expansions making use of the smallness of D and P with respect to l, gives an expression consistent with Eq. (17). For a simple pin hole with parallel detector and aperture the zeroth order term gives (cf. Ref. 18)

$$E(\bar{\xi}) \approx \frac{A_\mathrm{d} A_\mathrm{p}}{l^2} \cos^4(\bar{\xi} - \phi_\mathrm{d}), \tag{A3}$$

where A_d and A_p are the detector and aperture areas, respectively. If only the étendue $E(\xi)$ is required, and not the angular étendue or the geometric function, it can be more convenient to obtain the étendue by integrating the solid angle spanned by the aperture over the detector. It should be noted that, in general, we are interested in the étendue $E(\bar{\xi})$, so that the integral should be over a plane perpendicular to $\bar{\xi}$, and not over the detector. Realising that $k(p,\xi)$ is only a function of p and ξ, $E(\bar{\xi})$ can still be calculated by an integral over the detector:

$$E(\bar{\xi}) = \iint k(p(d),\xi) \frac{\cos(\xi - \phi_\mathrm{d})}{\cos(\xi - \bar{\xi})} \mathrm{d}d \, \mathrm{d}\xi,$$

where d is the coordinate along the detector surface in the xy plane, $p(d)$ is the p of the line (p,ξ) that intersects the detector at d, and the factor $\cos(\xi - \phi_\mathrm{d})$ arises due to geometrical considerations.

With the $k(p,\xi)$ from Eq. (A2) the geometric function in reconstruction space can be calculated by Eq. (8). Again the integrand is rather complicated and may only be solvable numerically. If, however, the same approximations are valid as the ones that led to Eq. (A3), $k(p,\xi)$ will be approximately constant and Eq. (9) can be used to calculate an approximation of the geometric function in reconstruction space analytically.

APPENDIX B: BEAM-WIDTH EFFECTS IN THE CORMACK METHOD

In the Cormack method[18,22] $f(p,\xi)$ is expanded in

$$f(p,\phi)=\sum_{m=0}^{\infty}\sum_{l=0}^{\infty}a_{ml}\,b_{ml}(p,\phi),$$

where $\phi=\xi+\pi/2$ ($\phi=[0,2\pi]$, and $p>0$), and the basis functions *in projection space* are

$$b_{ml}(p,\phi)=\frac{2}{m+2l+1}U_{m+2l+1}\left(\frac{p}{a}\right)\mathrm{e}^{im\phi},$$

where U_n are Chebyshev functions of the second kind. These basis functions in projection space correspond to global basis functions in (x,y) space:

$$[R^{-1}b_{ml}](r,\theta)=R_{ml}\left(\frac{r}{a}\right)e^{im\theta}, \tag{B1}$$

where R_{ml} are Zernike polynomials and (r,θ) are polar coordinates of (x,y).

With the help of Eq.(7), a measurement can be written as

$$\begin{aligned}\hat{f}_i&=\int_0^{2\pi}\int_0^{\infty}k_i(p,\phi)\,f(p,\phi)\,\mathrm{d}p\,\mathrm{d}\phi\\&=\sum_{m=0}^{\infty}\sum_{l=0}^{\infty}a_{ml}\int_0^{2\pi}\int_0^{\infty}k_i(p,\phi)\,b_{ml}(p,\phi)\,\mathrm{d}p\,\mathrm{d}\phi=\sum_{m=0}^{\infty}\sum_{l=0}^{\infty}a_{ml}B_{mli}.\end{aligned} \tag{B2}$$

The integrals and summations may be swapped since the b_{ml} are bounded on the integration interval and the series converges. In Eq. (B2) the beam-width effects are taken into account in the new basis functions B_{mli}, which can be calculated *a priori* and do not depend on the measurements or the emission profile. The tomographic reconstruction is obtained by solving the coefficients a_{ml} for a limited number of m and l from Eq. (B2). Multiplying Eq. (B1) by a_{ml} and summing over all m and l gives the tomogram.

APPENDIX C: BEAM-WIDTH EFFECTS IN THE IPR METHOD

In the Iterative Projection-space Reconstruction (IPR) method[23] the sinogram is approximated by an expansion into basis functions $b_m(p,\xi)$ in projection space that represent a bi-linear interpolation between regular grid points (or higher order interpolations), i.e.

$$f(p.\xi) \approx \sum_m b_m(p,\xi)\, f_m^{\mathrm{r}}, \tag{C1}$$

where f_m^{r} are the sinogram values in the regular grid points in projection space [location (p_m,ξ_m)] and

$$b_m(p,\xi) = t_p(p,p_m)\, t_\xi(\xi,\xi_m),$$

with

$$t_z(z,z_c) = \begin{cases} 0 & \text{if } z < z_c - \Delta z, \\ \dfrac{z - z_c + \Delta z}{\Delta z} & \text{if } z_c - \Delta z \le z < z_c, \\ \dfrac{z_c + \Delta z - z}{\Delta z} & \text{if } z_c \le z < z_c + \Delta z, \\ 0 & \text{if } z \ge z_c + \Delta z, \end{cases}$$

where z is p or ξ, and Δp and $\Delta\xi$ indicate the grid size.

In the original IPR method[23] the measurements are scaled iteratively to line-integral values f_i^{d} by means of Eq. (21), making use of tomograms reconstructed in previous iterations, after which the values f_m^{r} in regular grid points are reconstructed from these values f_i^{d} in irregular points by solving the system of equations

$$f_i^{\mathrm{d}} = \sum_m a_{im}\, f_m^{\mathrm{r}}, \tag{C2}$$

where $a_{im} = b_m(p_i,\xi_i)$. The tomogram is then obtained by tomographically inverting the values f_m^{r} in regular grid points by standard tomography methods.

In a way very similar to the case of the Cormack method (Appendix B) the beam-width effects can be included. Making use of Eq. (C1), we can write

$$\begin{aligned} \hat{f}_i &= \iint k_i(p,\xi)\, f(p,\xi)\,\mathrm{d}p\,\mathrm{d}\xi = \iint k_i(p,\xi)\Big[\sum_m b_m(p,\xi)\, f_m^{\mathrm{r}}\Big]\mathrm{d}p\,\mathrm{d}\xi \\ &= \sum_m f_m^{\mathrm{r}} \iint k_i(p,\xi)\, b_m(p,\xi)\,\mathrm{d}p\,\mathrm{d}\xi = \sum_m B_{im}\, f_m^{\mathrm{r}}, \end{aligned} \tag{C3}$$

which replaces Eq. (C2), and where $B_{im} = \iint k_i(p,\xi)\, b_m(p,\xi)\,\mathrm{d}p\,\mathrm{d}\xi$ can be calculated *a priori* and does not depend on the measurements or the emission profile. Therefore, the (approximate)

scaling to line-integral values of the original IPR method can be avoided and the full beam-width effects can be included by means of the coefficients B_{im}.

The main aim of the IPR method is to make it possible to make tomographic reconstructions from measurements by systems with an irregular coverage in projection space. Equation (C3) shows that it may even be useful to use the IPR method from an already regular coverage to include the beam-width effects. This is possible if the approximation by Eq. (C1) is adequate. This also demonstrates the similarity between taking into account the beam widths by Eq. (C3) and by the simplified method of Seq. 3.C.

APPENDIX D: ORTHOGONAL COORDINATES ON APERTURE CURVE

It is possible to construct curvilinear coordinates d and t in projection space that are locally perpendicular and parallel to the aperture curve of a given aperture. To be able to define an inner product, we have to make the dimensions of p and ξ equal, for example by normalizing p to a. Here, we normalize all spatial parameters to a. The choice of a is arbitrary [it depends, for example, on the origin (x_0, y_0)], and therefore the constructed coordinates d and t are, to a certain extent, arbitrary as well. We choose an aperture with the geometry as in Fig. 7(a).

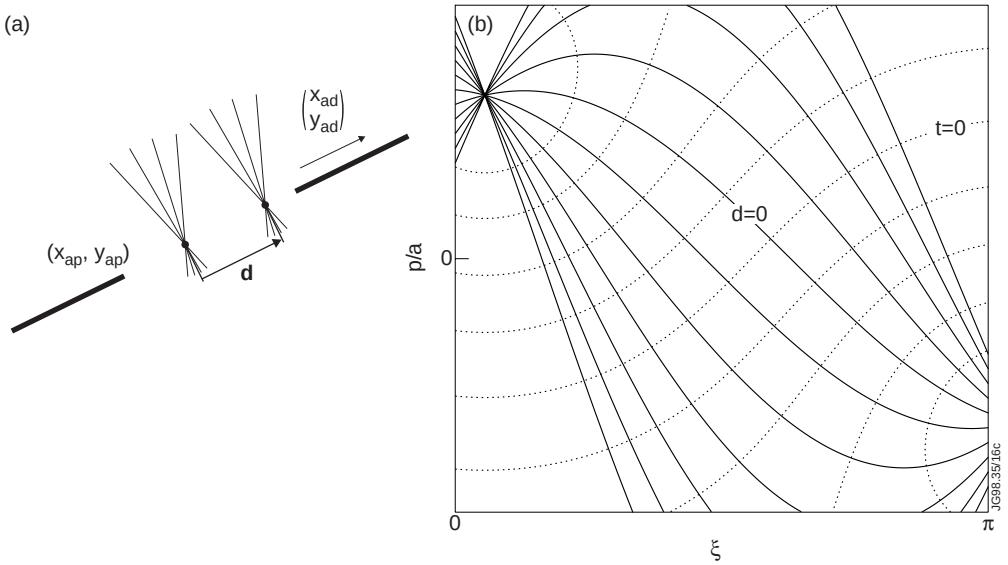

Figure 7. *(a) Geometry in* xy *plane of the pin-hole system discussed in Appendix D. Several lines of sight (thin lines) for two* $d =$ const *are shown. (b) Example of a number of curves* $d =$ const *(solid lines,* d *spaced equi-distantly) and* $t =$ const *(dashed lines) in projection space.*

As coordinate d we choose the signed distance between the centre of the aperture $(x_{\mathrm{ap}}, y_{\mathrm{ap}})$ and the intersection of the lines (p, ξ) with the aperture:

$$d(p,\xi) = \frac{p + x_{\mathrm{ap}} \sin\xi - y_{\mathrm{ap}} \cos\xi}{-x_{\mathrm{ad}} \sin\xi + y_{\mathrm{ad}} \cos\xi}. \tag{D1}$$

A number of curves $d = \mathrm{const}$ are shown in Fig. 7(b). The curve with $d = 0$ corresponds to the aperture curve of Eq. (23). A singularity for ξ parallel to $(x_{\mathrm{ad}}, y_{\mathrm{ad}})$ is apparent, which means that we can only define these curvilinear coordinates locally (the ξ at which the singularity occurs is far away from the range of ξ that is of interest).

Requiring global orthogonality, i.e. $\nabla_{p,\xi} d \cdot \nabla_{p,\xi} t = 0$ for all (p,ξ), one can construct

$$\begin{aligned} t(p,\xi) &= C_1(-x_{\mathrm{ad}}\cos\xi - y_{\mathrm{ad}}\sin\xi)\exp\left(-\frac{p^2}{2}\right) + C_1(x_{\mathrm{ap}}y_{\mathrm{da}} - y_{\mathrm{ap}}x_{\mathrm{da}})\int_{C_2}^{p}\exp\left(-\frac{u^2}{2}\right)\mathrm{d}u \\ &= (-x_{\mathrm{ad}}\cos\xi - y_{\mathrm{ad}}\sin\xi)\exp\left(-\frac{p^2}{2}\right) + \sqrt{\tfrac{\pi}{2}}(x_{\mathrm{ap}}y_{\mathrm{da}} - y_{\mathrm{ap}}x_{\mathrm{da}})\,\mathrm{erf}\left(\frac{p}{\sqrt{2}}\right), \end{aligned} \tag{D2}$$

where C_1 and C_2 are constants of integration that have been set to one and zero, respectively, in the final expression. A number of curves $t = \mathrm{const}$ are shown in Fig. 7(b).

It may be difficult to obtain closed expressions for $p(d,t)$ and $\xi(d,t)$, but for given d and t the p and ξ can be solved numerically from Eqs. (D1) and (D2). These, and the Jacobian of the coordinate transform, are required to change the integrals of Eq. (22) to d and t integrals.

APPENDIX E: COEFFICIENTS OF SIMPLIFIED METHOD

The coefficients of Eq. (25) of the simplified method are derived. See Smeulders[25] for an alternative derivation. It is assumed that through any three neighbouring points of a fan a sinogram curve $f(t) = a\,t^2 + bt + c$ can be fitted. For the point i and its neighbours one obtains the system of equations

$$\begin{cases} f(t_i) = a_i t_i^2 + b_i t_i + c_i = f_i, \\ f(t_{i+1}) = a_i t_{i+1}^2 + b_i t_{i+1} + c_i = f_{i+1}, \\ f(t_{i-1}) = a_i t_{i-1}^2 + b_i t_{i-1} + c_i = f_{i-1}. \end{cases}$$

For known f_{i-1}, f_i, and f_{i+1} one can solve a_i, b_i, and c_i, and express these in linear equations as follows

$$\begin{aligned} a_i &= \alpha_{ii} f_i + \alpha_{ii+1} f_{i+1} + \alpha_{ii-1} f_{i-1}, \\ b_i &= \beta_{ii} f_i + \beta_{ii+1} f_{i+1} + \beta_{ii-1} f_{i-1}, \\ c_i &= \gamma_{ii} f_i + \gamma_{ii+1} f_{i+1} + \gamma_{ii-1} f_{i-1}, \end{aligned}$$

where

$$\alpha_{ii} = \frac{t_{i+1} - t_{i-1}}{n_{a_i}},\ \alpha_{ii+1} = \frac{t_{i-1} - t_i}{n_{a_i}},\ \alpha_{ii-1} = \frac{t_i - t_{i+1}}{n_{a_i}},$$

with $$n_{a_i} = (t_i^2 - t_{i+1}^2)(t_i - t_{i-1}) - (t_i^2 - t_{i-1}^2)(t_i - t_{i+1}),$$

$$\beta_{ii} = \frac{2 + \alpha_{ii} n_{\alpha,b_i}}{n_{b_i}},\ \beta_{ii+1} = \frac{\alpha_{ii+1} n_{\alpha,b_i} - 1}{n_{b_i}},\ \beta_{ii-1} = \frac{\alpha_{ii-1} n_{\alpha,b_i} - 1}{n_{b_i}},$$

with $n_{b_i} = 2t_i - t_{i+1} - t_{i-1}$ and $n_{\alpha,b_i} = 2t_i^2 - t_{i+1}^2 - t_{i-1}^2$, and

$$\gamma_{ii} = \frac{1 - \alpha_{ii} n_{\alpha,c_i} - \beta_{ii} n_{\beta,c_i}}{n_{c_i}},\ \gamma_{ii+1} = \frac{1 - \alpha_{ii+1} n_{\alpha,c_i} - \beta_{ii+1} n_{\beta,c_i}}{n_{c_i}},\ \gamma_{ii-1} = \frac{1 - \alpha_{ii-1} n_{\alpha,c_i} - \beta_{ii-1} n_{\beta,c_i}}{n_{c_i}},$$

with $n_{c_i} = 3$, $n_{\alpha,c_i} = t_i^2 + t_{i+1}^2 + t_{i-1}^2$, and $n_{\beta,c_i} = t_i + t_{i+1} + t_{i-1}$. For the channels at the edges of the fan appropriate formulae can be obtained by replacing $i-1$ by $i+2$, and $i+1$ by $i-2$ for the respective channels.

If we express the integrals as

$$A_i = \int t^2 e_i(t)\,\mathrm{d}t,\ \ B_i = \int t e_i(t)\,\mathrm{d}t,\ \text{and}\ \ C_i = \int e_i(t)\,\mathrm{d}t,$$

then the coefficients of Eq. (25) for detector *i* can be expressed as

$$q_{ii} = \alpha_{ii} A_i + \beta_{ii} B_i + \gamma_{ii} C_i ,$$
$$q_{ii+1} = \alpha_{ii+1} A_i + \beta_{ii+1} B_i + \gamma_{ii-1} C_i ,$$
$$q_{ii-1} = \alpha_{ii-1} A_i + \beta_{ii-1} B_i + \gamma_{ii-1} C_i .$$

REFERENCES

1. R.N. Bracewell, "Correction for collimator width (restoration) in reconstructive x-ray tomography," J. Comp. Ass. Tomography **1**, 6–15 (1977)
2. B.M.W. Tsui and G.T. Gullberg, "The geometric transfer function for cone and fan beam collimators," Phys. Med. Biol. **35**, 81–93 (1990)
3. C.E. Metz, F.B. Atkins and R.N. Beck, "The geometric transfer function component for scintillation camera collimators with straight parallel holes," Phys. Med. Biol. **25**, 1059–1070 (1980)
4. S. Miracle, M.J. Yzuel, and S. Millán, "A study of the Point Spread Function in scintillation camera collimators based on Fourier analysis," Phys. Med. Biol. **24**, 372–384 (1979)
5. G.L. Zeng, G.T. Gullberg, B.M.W. Tsui, and J.A. Terry, "Three-dimensional iterative reconstruction algorithms with attenuation and geometric point response correction," IEEE Trans. Nucl. Sci. **38**, 693–702 (1991)
6. S.J. Glick, B.C. Penney, M.A. King, and C.L. Byrne, "Noniterative compensation for the distance-dependent detector response and photon attenuation in SPECT imaging," IEEE Trans. Med. Imaging **13**, 363–374 (1994)
7. A.R. Formiconi, A. Pupi, and A. Passeri, "Compensation of spatial system response in SPECT with conjugate gradient reconstruction technique," Phys. Med. Biol. **34**, 69–84 (1989)
8. R.M. Lewitt, P.R. Edholm and W. Xia, "Fourier method for correction of depth-dependent blurring," SPIE Vol. 1092 *Medical Imaging III, Image Processing* (1989), pp. 232-243
9. R.H.T. Bates and M.J. McDonnell, *Image restoration and reconstruction* (Clarendon Press, Oxford, 1986), pp. 133
10. R. Reichle *et al.*, "Bolometer for ITER," in *Diagnostics for experimental thermonuclear fusion reactors*, Eds. P.E. Stott *et al*. (Plenum Press, New York,1996), pp. 560-569 and references therein
11. S.R. Deans, *The Radon transform and some of its application* (Wiley, New York, 1983)
12. J.L. Prince and A.S. Willsky, "A geometric projection-space reconstruction algorithm," Linear Algebra and Its Applications **130**, 151–191 (1990)
13. G.T. Herman, *Image reconstructions from projections* (Academic Press, New York, 1980), p. 98

14. R.M. Lewitt, “Reconstruction algorithms: transform methods,” Proc. IEEE **71**, 390–408 (1983)
15. V.V. Pikalov and N.G. Preobrazhenskii, “Computer-aided tomography and physical experiment,” Sov. Phys. Usp. **26**, 974-990 (1984)
16. R.S. Longhurst, *Geometrical and physical optics (third edition)* (Longman, Harlow, 1973), p. 20, 450, 466
17. L.C. Ingesson, *Visible-light tomography of tokamak plasmas* (Thesis Technische Universiteit Eindhoven, The Netherlands, 1995)
18. R.S. Granetz and P. Smeulders, “X-ray tomography at JET,” Nucl. Fusion **28**, 457–476 (1988)
19. J.F. Camacho, *Soft x-ray tomography on the Alcator C tokamak*, Report PFC/RR-85-11 (Massachusetts Institute of Technology, 1985)
20. C.P. Tanzi, *Emission of soft x-ray and microwave radiation from tokamak plasmas*, (Thesis Universiteit Utrecht, The Netherlands, 1996), pp. 68
21. L.C. Ingesson *et al.*, “Soft x-ray tomography during ELMs and impurity injection in JET,” submitted to Nucl. Fusion
22. A.M. Cormack, “Representation of a function by its line integrals, with some radiological applications. II,” J. Appl. Phys. **35**, 2908–2913 (1964)
23. L.C. Ingesson and V.V. Pickalov, “An iterative projection-space reconstruction algorithm for tomography systems with irregular coverage,” J. Phys. D: Appl. Phys. **29**, 3009–3016 (1996)
24. M.R. Teague, “Image analysis via the general theory of moments,” J. Opt. Soc. Am. **20**, 920–930 (1980)
25. P. Smeulders, *Second order Abel inversion with allowance for the spatial resolution*, Report IPP 2/240 (Max-Planck-Institut für Plasmaphysik, Garching, Germany, 1978)
26. P. Smeulders, *A fast plasma tomography routine with second-order accuracy and compensation for spatial resolution*, Report IPP 2/252 (Max-Planck-Institut für Plasmaphysik, Garching, Germany, 1983)
27. L.C. Ingesson *et al.*, “Radiation distribution and neutral-particle loss in the JET MkI and MkIIA divertors,” in *Proceedings of the 24th EPS conference on Controlled Fusion and Plasma Physics*, Berchtesgaden, 9–13 June 1997, Ed. M. Schittenhelm *et al.*, Europhysics Conference Abstracts Vol. 21A, (EPS, 1997) Part I, pp. 113-116